

Emergent Conformal Symmetry at the Multicritical Point of (2+1)D SO(5) Model with Wess-Zumino-Witten Term on Sphere

Bin-Bin Chen,¹ Xu Zhang,¹ and Zi Yang Meng^{1,*}

¹*Department of Physics and HKU-UCAS Joint Institute of Theoretical and Computational Physics,
The University of Hong Kong, Pokfulam Road, Hong Kong SAR, China*

(Dated: May 16, 2024)

Novel critical phenomena beyond the Landau-Ginzburg-Wilson paradigm have been long sought after. Among many candidate scenarios, the deconfined quantum critical point (DQCP) constitutes the most fascinating one, and its lattice model realization has been debated over the past two decades. Following the pioneering works with the fuzzy sphere methods [1–4], we apply the spherical Landau level regularization to study the effective (2+1)D SO(5) non-linear sigma model with a topological term and the potential DQCP therein. Utilizing the state-of-the-art density matrix renormalization group method with explicit $SU(2)_{\text{spin}} \times U(1)_{\text{charge}} \times U(1)_{\text{angular-momentum}}$ symmetry as well as exact diagonalization simulations, we provide a comprehensive phase diagram for the model with a SO(5) continuous transition line — extension of the previous identified SO(5) multicritical point [5] — while tuning interaction length. The state-operator correspondence with the conformal tower structure is used to identify the emergent conformal symmetry with the best scaling dimension of relevant primary fields and they match well with the critical exponents obtained from the crossing point analysis of the correlation ratio. Our results thus further support the rich structure of the phase diagram of the SO(5) model.

Introduction.— Novel critical phenomena beyond Landau-Ginzburg-Wilson paradigm can fundamentally enrich our understanding to the phase transitions of highly entangled quantum matter. Amongst many, the deconfined quantum criticality, known as the direct continuous transition between two spontaneous symmetry-broken states, has been long-sought-after [6–10]. However, the initial proposed lattice realizations [11, 12], i.e. from Néel to valence bond solid (VBS) transition in J - Q spin model, with drifting critical exponents are incompatible with conformal bootstrap bounds [13–18], has been shown to exhibit weakly first-order transition behavior, over the years of heroic efforts [13, 14, 19–22]. It can turn into a continuous transition—a real DQCP—at least when $N > 8$ in the $SU(N)$ version of J_1 - J_2 spin model [23–26]. At the large N limit, the transition is believed to be described by the Abelian Higgs theory with unitary conformal fixed point [27–29].

The obstacles of finding a DQCP in the realistic $SU(2)$ setting originate from the symmetry emergence requirement. To be specific, in the $SU(2)$ version of J - Q model on square lattice, a $U(1)$ symmetry is firstly required to emerge from the \mathbb{Z}_4 symmetry in the VBS phase around the transition point [11]. However, such $U(1)$ symmetry emergence is subtle due to the dangerously irrelevant perturbation (the monopole event) [15, 17]: the $U(1)$ is emergent only in the infrared limit, while in contrast the \mathbb{Z}_4 symmetry breaking term is relevant, which obscures the numerical analysis when an additional \mathbb{Z}_4 symmetry length scale is approached. Furthermore, the emerged $U(1)$ symmetry in the VBS phase should again combine with the $SU(2)$ symmetry in the Néel phase to give rise to a final SO(5) symmetry [30]. Such symmetry emergence

requirement might set up a high bar for realizing SO(5) in lattice models, where a slow renormalization group (RG) flow may cause considerable finite-size effect, and eventually lead to the observation of the weakly first order transition after years of accumulating works.

Given the situation, an explicit SO(5) model with Wess-Zumino-Witten (WZW) topological term by projecting fermion density-density interaction on the Landau level is proposed to circumvent such symmetry emergence requirement in the Néel-VBS lattice models [31]. Such a model has been numerically visited on both torus [32, 33] and recently spherical geometries [4, 5]. As pointed out in the seminal works of Refs. [1–4], the advantage of the spherical geometry is to directly expose the underlying conformal field theory (CFT) algebra and operator content, since for a Hamiltonian living on $S^{d-1} \times R$ space-time geometry, the scaling dimensions of CFT operators has one-to-one correspondence with the eigenenergies of CFT states, dubbed as the state-operator correspondence [34–36]. Recently, by using the idea of the spherical regularization [37, 38], the conformal data including the scaling dimensions and operator product expansion (OPE) coefficients have been characterised in the (2+1)D Ising [1, 2], O(3) critical points [3], and SO(5) pseudo-criticality [4] (we also note an conformal perturbation theory approach in Ising [39] and O(2) cases [40]). The conformal defect can also be studied with the fuzzy sphere regularization [41, 42].

In our previous work of SO(5) model on sphere [5], we mapped out the phase diagram of the model, not only along the SO(5) symmetric line but also break the symmetry down to $SO(3) \times SO(2)$, and probe all the possible symmetry-breaking phases therein. We find a possible gapless SO(5) symmetric phase separating the Néel

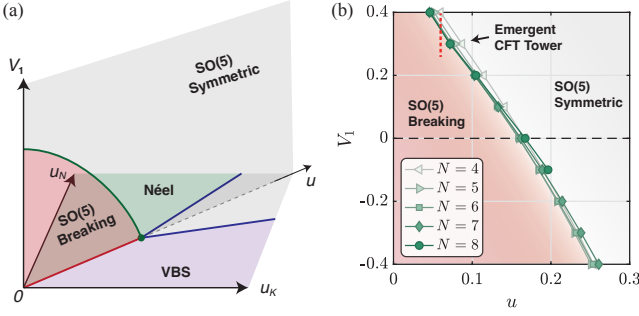


FIG. 1. **Global phase diagram of the SO(5) model.** (a) The u_K - u_N plane is obtained from our previous work [5], where tuning along the u axis respects the SO(5) symmetry. We found a multicritical point (the green dot) separating the SO(5) symmetry-breaking line (the red segment) and a SO(5) symmetric phase which further separates the Néel (green) and VBS (blue) phases. In this work, we extend the interaction to longer range by adding the V_1 term in the Hamiltonian (preserve the SO(5) symmetry), which allows us to scan the u - V_1 plane to look for the transition point between SO(5) breaking and SO(5) symmetric phases with the emergent CFT structure. (b) Obtained phase boundary in the u - V_1 plane by identifying the calibrated scaling dimension $\Delta_{\mathcal{T}^{\mu\nu}} = 3$. One sees the boundary is converged with $N = 6$ near the black arrow where the emergent CFT structure is discovered close to $V_1 = 0.3$. The red dashed line indicates the DMRG simulations in Fig. 4 where the critical point and scaling dimension from finite size crossing point analysis are consistent with the CFT spectrum results.

and VBS phases, and the transitions from the symmetric phase towards Néel and VBS symmetry breaking phases acquire non-Wilson-Fisher critical exponents. More importantly, these two phase boundaries meet at a multicritical point below which the SO(5) symmetry is spontaneously broken and the Néel-VBS transition becomes first-order. Our results are consistent with recent understanding that the aforementioned Néel-VBS weakly first-order transition [13, 14, 19–22, 25, 26] is located close but below our multicritical point, and the recent conformal bootstrap analysis of deconfined quantum tricriticality [43]. However, the precise critical exponents are hard to derive there because of the still relatively large finite size effect [4, 5]. One would need to further fine-tune the Hamiltonian (preserving SO(5) symmetry) to fully review the emergent conformal symmetry structure at the multicritical point within reachable sizes of such spherical setting.

In this work, we accomplish this goal by extending the interaction length of the Hamiltonian, which allows us to search for a group of parameters with smaller finite-size effect in the enlarged parameter space, where irrelevant operators are sufficiently suppressed. Such prescription has been successfully applied to the studies in the 3D Ising and O(3) transitions in fuzzy sphere method [1–3]. With that parameters, several low-lying primary opera-

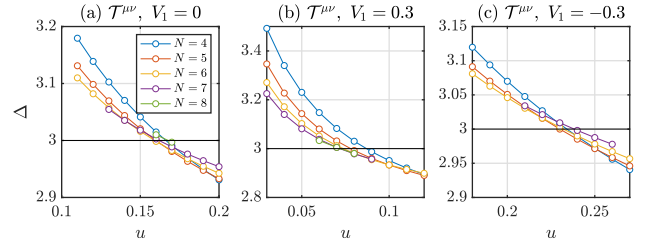


FIG. 2. **Scaling dimension of stress tensor $\Delta_{\mathcal{T}^{\mu\nu}}$.** Calibrated by $\Delta_{J^\mu} = 2$, $\Delta_{\mathcal{T}^{\mu\nu}}$'s are shown versus u/U_0 for different system sizes $N = 4, 5, 6, 7, 8$, for different interaction strength (a) $V_1 = 0$, (b) $V_1 = 0.3$, and (c) $V_1 = -0.3$. The $\Delta_{\mathcal{T}^{\mu\nu}} = 3$ criterion determines the transition point for each V_1 .

tors show perfectly conformal tower structure indicating a CFT here. The phase transition point and scaling dimension of order parameter from finite-size crossing point analysis of the SO(5) correlation ratio [5, 8, 15, 44–46], match well with the conformal tower results. This self-consistence check indicates the robustness of our conclusion. Our results provide a strong evidence for the conformal symmetry of the multicritical SO(5) CFT fixed point, which separates the SO(5) symmetry-breaking first-order transition line and the SO(5) symmetric phase in the global phase diagram of the model (Fig. 1), and it is from this multicritical point the non-Wilson-Fisher phase boundaries between the symmetric to Néel and VBS phases are originated.

Model and Methods.— We consider the (2+1)D Hamiltonian $H_\Gamma = \int d\mathbf{r}_1 d\mathbf{r}_2 U(\mathbf{r}_1, \mathbf{r}_2) [n^0(\mathbf{r}_1)n^0(\mathbf{r}_2) - \sum_{i=1}^5 u_i n^i(\mathbf{r}_1)n^i(\mathbf{r}_2)]$, where $n^i(\mathbf{r}) = \Psi(\mathbf{r})^\dagger \Gamma^i \Psi(\mathbf{r}) - 2\delta_{i0}$ is a local density operator with $\Psi(\mathbf{r}) \equiv \psi_{\tau\sigma}(\mathbf{r})$ the 4-component Dirac fermion annihilation operator with mixing valley τ and spin σ indices. Here $\Gamma^0 = \mathbb{I} \otimes \mathbb{I}$ is the identity matrix and $\{\Gamma^1, \dots, \Gamma^5\} = \{\tau_x \otimes \mathbb{I}, \tau_y \otimes \mathbb{I}, \tau_z \otimes \sigma_x, \tau_z \otimes \sigma_y, \tau_z \otimes \sigma_z\}$ are the 5 mutually anticommuting matrices of the SO(5) group. The short-range density-density interaction is $U(\mathbf{r}_1, \mathbf{r}_2) = \frac{g_0}{R^2} \delta(|\mathbf{r}_1 - \mathbf{r}_2|) + \frac{g_1}{R^4} \nabla^2 \delta(|\mathbf{r}_1 - \mathbf{r}_2|)$ where g_1 is used to tune the interaction length. In previous works [4, 5], only a purely local interaction is considered with $g_1 = 0$.

Subsequently, we project the SO(5) Dirac fermion Hamiltonian onto the zero energy Landau level on the sphere, which is the same as the massive fermion lowest Landau levels (LLL) of a sphere with $4\pi s$ magnetic monopole at its origin [37, 38, 47, 48], where the $(2s+1)$ -fold degenerate LLL wavefunction takes the form of $\Phi_m(\Omega) \propto e^{im\phi} \cos^{s+m}(\frac{\theta}{2}) \sin^{s-m}(\frac{\theta}{2})$ with $m \in \{-s, -s+1, \dots, s-1, s\}$ and $2s \in \mathbb{Z}$. By enlarging s one can effectively enlarge the surface (system size) of the sphere while keeping the local magnetic field on the surface unchanged. After projection $\psi(\Omega) \rightarrow \sum_m \Phi_m(\Omega) c_m$,

one can derive the projected Hamiltonian

$$\begin{aligned}\hat{H}_\Gamma^{(LLL)} &= \hat{H}_0 - \sum_{i=1}^5 u_i \hat{H}_i, \text{ with} \\ \hat{H}_{i \in \{0,1,\dots,5\}} &= \sum_{m_1, m_2, m} V_{m_1, m_2, m_2-m, m_1+m} \times \\ &\quad (c_{m_1}^\dagger \Gamma^i c_{m_1+m} - 2\delta_{i0} \delta_{m0}) (c_{m_2}^\dagger \Gamma^i c_{m_2-m} - 2\delta_{i0} \delta_{m0})\end{aligned}\quad (1)$$

where V_{m_1, m_2, m_3, m_4} is connected to the Haldane pseudo-potential V_l by $V_{m_1, m_2, m_3, m_4} = \sum_l V_l (4s - 2l + 1) \begin{pmatrix} s & s & 2s-l \\ m_1 & m_2 & -m_1-m_2 \end{pmatrix} \begin{pmatrix} s & s & 2s-l \\ m_4 & m_3 & -m_3-m_4 \end{pmatrix}$. For the considered short-range interaction here, only V_0 and V_1 are involved in the above l -summation [c.f. Supplemental Material (SM) for the relation between (g_0, g_1) and (V_0, V_1) [49]]. This model is known to be described by a SO(5) non-linear sigma model with a WZW term [31–33]. We define $u_K = u_1 = u_2$ for the VBS control parameter, and $u_N = u_3 = u_4 = u_5$ for the Néel control parameter. Throughout this work, we set $V_0 = 1$ as the energy unit and focus on the SO(5) case, i.e. $u = u_K = u_N$ while tuning u (distance from SU(4) fixed point) and V_1 (finite-length interaction strength) to reduce the finite size effect of the SO(5) phase boundary found in our previous work [5]. Details of the spherical regulation is given in SM [49]. We note this approach is used in Ref. [4] to propose the pseudo-criticality along the $u_K = u_N$ SO(5) line.

In this work, we employ density matrix renormalization group (DMRG) method with $\text{SU}(2)_{\text{spin}} \times \text{U}(1)_{\text{charge}} \times \text{U}(1)_{\text{angular-momentum}}$ symmetry, and exact diagonalization (ED), to accurately determine the phases and their phase boundaries. In our DMRG simulations, the SU(2) symmetry is implemented in the framework of the tensor library QSpace [50–52], with up to 4096 SU(2) invariant multiplets (equivalent to ~ 12000 U(1) states) kept to render the truncation errors within 5×10^{-5} . We denote the system size by the Landau level degeneracy $N = 2s + 1$ and obtain converging results with $N = 3, 4, 5, \dots, 12$ to control finite size scaling behavior. In the energy level computation, we exploit ED for $N = 4, 5, \dots, 7$ and DMRG for $N = 8$.

Phase Diagram and the SO(5) phase transition.— We first give a summary of the phase diagram. As shown in Fig. 1 (a), for the case of $V_1 = 0$, the $u_K - u_N$ plane of the phase diagram is investigated in our previous work [5], where generically the SO(5) symmetry is split into SO(3) \times SO(2) symmetry and the Néel (green) and VBS (purple) phases are either separated by a direct first-order transition (solid red line) or through an intermediate symmetric phase (grey area). The SO(3) and SO(2) transition lines (solid blue line) merge into a fine-tuned multi-critical point (green dots) in the plane. Here, we will show that, in the SO(5) cases of $u_K = u_N = u$, by adding a V_1 axis, the multi-critical point further ex-

tends as a transition line separating the SO(5)-breaking (red area) and the SO(5)-symmetric phases.

To identify such SO(5) transition line, we resort to the state-operator correspondence, i.e., for a CFT operator O_k , the corresponding energy gaps $E_k - E_0$ are proportional to the scaling dimensions Δ_k , i.e., $E_k - E_0 = \frac{v}{R} \Delta_k$, where R is the radius of the sphere and v is a model-dependent velocity [53, 54]. To search for the potential SO(5) CFT points in the V_1 - u phase diagram, we need to firstly match the energy spectra of the considered SO(5) model with the operator spectrum, to be specific, determining the velocity v and to rescale the energy spectra with the factor v/R . Note that, the symmetry current J^μ and the energy-momentum tensor $\mathcal{T}^{\mu\nu}$ don't renormalize in perturbation theory, i.e. they have zero anomalous dimensions, meaning that their scaling dimensions $\Delta_{J^\mu} = d - 1 = 2$ and $\Delta_{\mathcal{T}^{\mu\nu}} = d = 3$ [35], which can serve as natural calibrators for the operator spectrum.

With the prescription established in 3D Ising transition [1, 2], O(3) Wilson-Fisher transition [3], and SO(5) pseudo-criticality [4], we rescale the energy spectrum by exactly setting $\Delta_{J^\mu} = 2$ and searching in the V_1 - u parameter space for $\Delta_{\mathcal{T}^{\mu\nu}} = 3$. This will determine a critical line which should coincide with the SO(5) phase boundary obtained from the correlation ratio data, as we will discuss in Fig. 4. As shown in Fig. 2, at the fixed $V_1 = 0, 0.3, -0.3$ cuts, we plot the scaling dimension of $\mathcal{T}^{\mu\nu}$ versus u for various system sizes $N = 4, 5, \dots, 8$. By collecting those $\Delta_{\mathcal{T}^{\mu\nu}} = 3$ points and we plot them as the phase boundary in Fig. 1 (b).

Energy spectrum evidence for conformal symmetry.— The finger-print evidence for the CFT nature is the integer-spaced tower structure of the primary operators and their descendant's [1]. That is, for scalar primary operator \hat{O} with scaling dimension Δ and Lorentz spin $l = 0$, its descendants express as $\partial_{\nu_1} \dots \partial_{\nu_m} \square^n \hat{O}$ with $m, n \geq 0$ whose scaling dimension will be $\Delta + 2n + m$, and the Lorentz spin will be m [34, 35]. Note that, for spin- l primary operator $O_{\mu_1 \dots \mu_l}$, e.g. the spin-1 current operator J^μ and the spin-2 stress tensor operator $\mathcal{T}^{\mu\nu}$, there are two types of descendants. The first type is expressed as

$$\partial_{\nu_1} \dots \partial_{\nu_m} \partial_{\mu_1} \dots \partial_{\mu_i} \square^n \hat{O}_{\mu_1 \dots \mu_l} \quad (2)$$

whose scaling dimension will be $\Delta + 2n + m + i$, and the Lorentz spin will be $l + m - i$. The second type can be expressed as

$$\epsilon_{\mu_1 \rho \tau} \partial_\rho \partial_{\nu_1} \dots \partial_{\nu_m} \partial_{\mu_1} \dots \partial_{\mu_i} \square^n \hat{O}_{\mu_1 \dots \mu_l} \quad (3)$$

whose scaling dimension will be $\Delta + 2n + m + i + 1$, and the Lorentz spin will be $l + m - i$. The ϵ tensor of SO(3) will alter spacetime parity symmetry of $\hat{O}_{\mu_1 \dots \mu_l}$. In addition, for conserved operators like J^μ and $\mathcal{T}^{\mu\nu}$, due to the conservation law $\partial_\mu J^\mu = 0$ and $\partial_\mu \mathcal{T}^{\mu\nu} = 0$, their descendants should have $i = 0$.

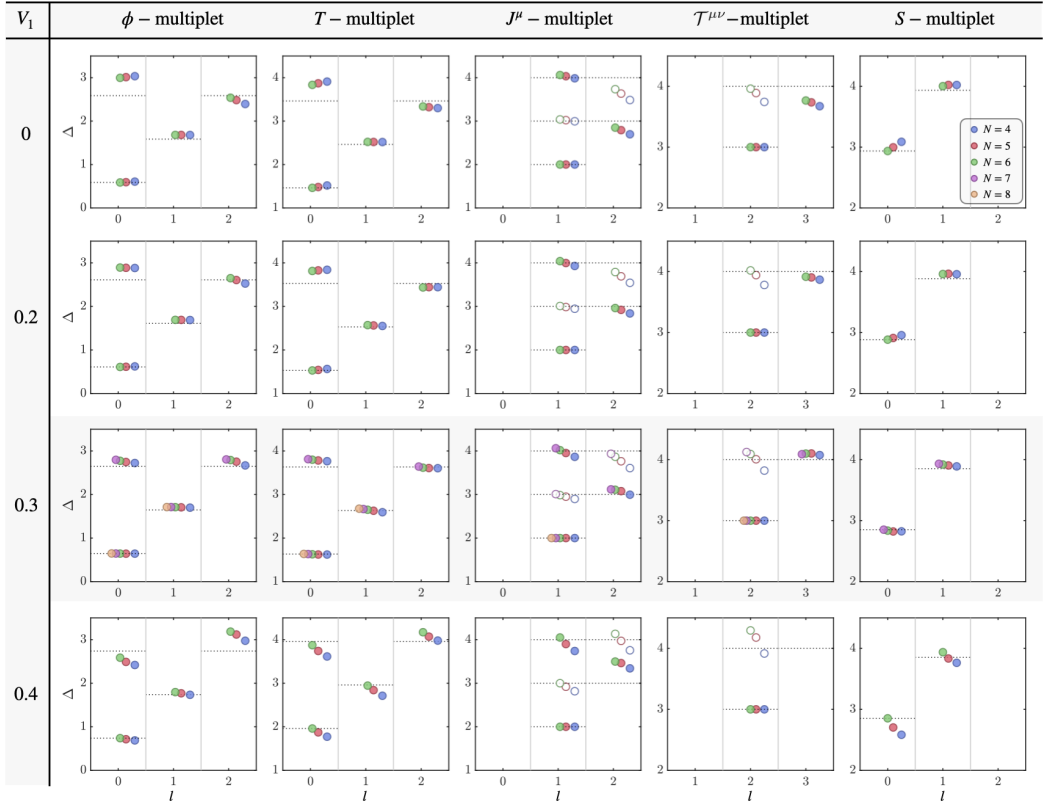


FIG. 3. **Conformal multiplets of several low-lying primary operators.** Scaling dimension Δ versus Lorentz spin l for the lowest vector ϕ (1st column), the lowest rank-2 symmetric traceless tensor T (2nd column), the conserved current J^μ (3rd column), the stress tensor $\mathcal{T}^{\mu\nu}$ (4th column) and the scalar (singlet operator) S (5th column), when tuning interacting $V_1 = 0$ (1st row), $V_1 = 0.2$ (2nd row), $V_1 = 0.3$ (3rd row), $V_1 = 0.4$ (4th row). Following the pioneering work of Ref. [4], the scaling dimensions Δ 's are calibrated by the scaling dimension of the conserved current $\Delta_{J^\mu} = 2$. We find the emergent CFT structure manifest close to $V_1 = 0.3$ (indicated by the grey background) and it represent the CFT of the SO(5) multicritical point. Here the solid/empty-filled circles depict the first/second type descendants [c.f. Eq. (2), Eq. (3)]. Note that, the first row ($V_1 = 0$) is consistent with the CFT spectrum observed in Ref. [4].

Due to finite size effect, the operator spectrum might lose such integer-space structure, and our second step is to suppress the irrelevant operators to expose the CFT tower in a small size simulation by tuning the parameter V_1 along the phase boundary, as has been employed in 3D Ising and O(3) transitions [1–3]. Here, we consider the SO(5) order parameter ϕ (the lowest vector representation), the lowest rank-2 symmetric traceless tensor T , the symmetry current J^μ , the stress tensor $\mathcal{T}^{\mu\nu}$, the SO(5) singlet operator S (the lowest scalar representation), as well as their descendant's. The degeneracy of these operators with their associated quantum numbers are explicitly given in the tensor representation of the SO(5) group in SM [49].

As shown in Fig. 3, we align the towers of different operators in separated columns, i.e., ϕ the first, T the second, J^μ the third, $\mathcal{T}^{\mu\nu}$ the fourth, and S the last column. The different rows indicate different interactions strength $V_1 = 0, 0.2, 0.3, 0.4$. We note, the first row ($V_1 = 0$) corresponds to the CFT spectrum observed in Ref. [4]. In

each plot, the operator spectrum with different Lorentz spin l is split by the vertical solid lines, and the horizontal dotted lines indicate the perfect integer-spaced tower structure. The numerical results for the first/second type descendants are depicted as solid/empty-filled circle in the plots. It can be clearly seen that, as V_1 increases, the CFT towers get increasingly well-behaved, i.e., each operator approaches to the corresponding integer-spaced horizontal line. At $V_1 = 0.3$, we find, the operator spectra recover the CFT towers up to second descendant operators. Further increase V_1 above 0.3, the structure disappear again. Therefore, we find close to $V_1 = 0.3$ and along the u scan, the finite size effect, i.e. the irrelevant operators, has been successfully removed.

Scaling dimensions of relevant operators.— Other than the above primary operators, i.e., ϕ, T, S , we also find another relevant operator, the 6π -monopole operator $M_{6\pi}$ whose scaling dimension is smaller than 3. As shown in Tab. I, we list all the relevant operators at $V_1 = 0.3$. Remarkably, we find that, the singlet operator S and

TABLE I. Scaling dimension of relevant primary operator at $V_1 = 0.3$ for various system sizes N .

Operators	N				
	4	5	6	7	8
ϕ	0.642	0.642	0.644	0.646	0.647
T	1.622	1.622	1.627	1.633	1.636
J^μ	2.000	2.000	2.000	2.000	2.000
S	2.853	2.823	2.873	2.884	—
$M_{6\pi}$	2.825	2.861	2.836	2.852	—
$\mathcal{T}^{\mu\nu}$	3.000	3.000	3.000	3.000	3.000

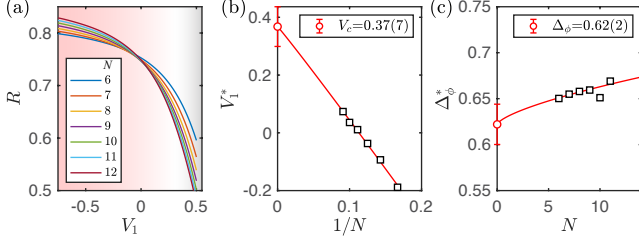


FIG. 4. **DMRG data for SO(5) transition.** (a) Correlation ratio R of SO(5) order parameter are shown versus V_1 at fixed $u = 0.06$. (b) The critical point is extrapolated from the finite-size crossing point V_c^* and yields $V_c = 0.37(7)$, consistent with the phase boundary in Fig. 1 (b). (c) The scaling dimension extrapolated to be $\Delta_\phi = 0.62(2)$ is also consistent with CFT spectrum in Tab. I.

the rank-2 tensor T possesses scaling dimensions $\Delta_S \simeq 2.884 < 3$ and $\Delta_T \simeq 1.636 < 3$ which means that the operator away from the SO(5) axis is relevant. That is, the observed SO(5) CFT is a multicritical point (in the $\text{SO}(3) \times \text{SO}(2)$ u_K - u_N plane) with two relevant singlet operators, the SO(5) singlets S and T (this singlet comes from decomposing T of SO(5) to $\text{SO}(3) \times \text{SO}(2)$ [43]), in consistence with the recent conformal bootstrap analysis of the deconfined quantum tricritical scenario [43]. We also note that, Ref. [4] obtained the similar dimensions $\Delta_S = 2.831$, $\Delta_T = 1.458$ while having different interpretation of pseudocriticality due to the vast region of CFT behaviour in the case of $V_1 = 0$, ruling out the possibility of a quantum transition therein. Here, as shown in the Fig. 1(b) that, the phase boundaries still vary slowly with system size N , which can be improved by increasing V_1 with well-converged phase boundaries around $V_1 = 0.3$, signaling the stabilization of the transition point and the validity of the fine-tuning multicriticality scenario.

As an important sanity check, we also determine the scaling dimension of the order parameter by calculating the correlation ratio of the SO(5) order parameter in DMRG [5]. For the SO(5) ordered phase, we define $O_{i,l,m} = \int d\mathbf{r} Y_{lm}^*(\mathbf{r}) \Psi^\dagger(\mathbf{r}) \Gamma^i \Psi(\mathbf{r})$ with $Y_{l,m}(\mathbf{r})$ being the spherical harmonic function, and compute the squared order parameter $m_l^2 = \frac{1}{N^2} \sum_{i=1}^5 \langle O_{i=1,l}^2 \rangle$ and the corresponding correlation ratio $R = 1 - m_{l=1}^2 / m_{l=0}^2$.

In Fig. 4 (a), we fix $u = 0.06$ and vary V_1 . The VBS correlation ratio R exhibits a nice crossing behaviour, which suggests the SO(5)-breaking phase at smaller V_1 and the symmetric phase at larger V_1 . As in our previous work [5], it can be seen that, the crossing points exhibit slightly drifting behaviour, which can be described by the scaling form $V_1^*(N, N+1) = V_c + N^{-\frac{1}{2\nu} - \frac{\omega}{2}}$ (the asterisk indicates the finite-size crossing points and the critical point in the thermodynamic limit is indicated by the subscript ‘c’). In Fig. 4 (b), we find the crossing points are best fitted by a linear form $V_1^* = a + b/N$, and obtain the critical point from the intercept $V_c = a = 0.37(7)$, consistent with the phase diagram in Fig. 1 (b). We then define $\Delta_\phi^*(N) = -N \log \frac{m^2(V_c, N+1)}{m^2(V_c, N)}$, which follows the scaling form $\Delta_\phi^*(N) = \Delta_\phi + aN^{\frac{1}{2\nu}}$. Here the exponent $\nu = \frac{1}{3-\Delta_T} \simeq 0.733$ is determined from the Δ_T in Tab. I. And as shown in Fig. 4 (c), the order parameter scaling dimension $\Delta_\phi = 0.62(2)$ is obtained, consistent with the CFT $\Delta_\phi = 0.647$ in Tab. I. Such consistency between the finite size crossing point analysis of the SO(5) correlation ratio and the CFT spectrum, in giving rise to the same transition point and the scaling dimension of the SO(5) order parameter, supports the analysis employed in Ref. [5] and can be extended to the entire phase diagram around the multicritical point.

Discussions.— Following the pioneering work of Ref. [4], our study provides a comprehensive phase diagram for the (2+1)D SO(5) non-linear sigma model with WZW term on a sphere, as well as the multicritical properties of the SO(5) transition. Our findings reveal the 3D SO(5) multicriticality by identifying the CFT tower structure when tuning irrelevant operators. These results, combined with recent observations of the weakly first transition in the SU(2) spin models with Néel-VBS transtions [13, 14, 19–22, 25, 26], provide a direction for the long-standing question on the existence of DQCP in various settings.

One of the remaining questions is the nature of the symmetric phase and its previously determined non-Wilson-Fisher transition towards the VBS and Néel phases once one departs from the SO(5) line [5]. A few possible CFT scenarios have already been proposed [55–58] that requires emergent \mathbb{Z}_2 or SU(2) gauge fields. We will present our analysis of these scenarios in a forthcoming work. Also, the relation of the multicriticality and the previously discovered pseudocriticality at $V_1 = 0$ [4] will be of interests to further explore. In addition, conformal perturbation theory [39] can also be applied to study the deviations from conformal spectrum in the future works.

Acknowledgment.— We thank Kai Sun, Yuxuan Wang, Meng Cheng, Cenke Xu, Wei Zhu, Yin-Chen He, Fakher Assaad, Anders Sandvik, Senthil Todadri, Slava Rychkov, Shai Chester, Subir Sachdev for valuable discussions on the related topic. We acknowledge the support from the Research Grants Council (RGC) of Hong

Kong Special Administrative Region of China (Project Nos. 17301721, AoE/P-701/20, 17309822, HKU C7037-22GF, 17302223), the ANR/RGC Joint Research Scheme sponsored by RGC of Hong Kong and French National Research Agency (Project No. A HKU703/22), the GD-NSF (No. 2022A1515011007) and the HKU Seed Funding for Strategic Interdisciplinary Research. We thank HPC2021 system under the Information Technology Services and the Blackbody HPC system at the Department of Physics, University of Hong Kong, as well as the Beijing PARATERA Tech CO.,Ltd. (URL: <https://cloud.paratera.com>) for providing HPC resources that have contributed to the research results reported within this paper.

* zymeng@hku.hk

- [1] W. Zhu, C. Han, E. Huffman, J. S. Hofmann, and Y.-C. He, Phys. Rev. X **13**, 021009 (2023).
- [2] L. Hu, Y.-C. He, and W. Zhu, Phys. Rev. Lett. **131**, 031601 (2023).
- [3] C. Han, L. Hu, and W. Zhu, arXiv e-prints, arXiv:2312.04047 (2023), arXiv:2312.04047 [cond-mat.str-el].
- [4] Z. Zhou, L. Hu, W. Zhu, and Y.-C. He, arXiv e-prints, arXiv:2306.16435 (2023), arXiv:2306.16435 [cond-mat.str-el].
- [5] B.-B. Chen, X. Zhang, Y. Wang, K. Sun, and Z. Y. Meng, arXiv e-prints, arXiv:2307.05307 (2023), arXiv:2307.05307 [cond-mat.str-el].
- [6] T. Senthil, L. Balents, S. Sachdev, A. Vishwanath, and M. P. A. Fisher, Phys. Rev. B **70**, 144407 (2004).
- [7] C. Wang, A. Nahum, M. A. Metlitski, C. Xu, and T. Senthil, Phys. Rev. X **7**, 031051 (2017).
- [8] Y. Q. Qin, Y.-Y. He, Y.-Z. You, Z.-Y. Lu, A. Sen, A. W. Sandvik, C. Xu, and Z. Y. Meng, Phys. Rev. X **7**, 031052 (2017).
- [9] N. Ma, G.-Y. Sun, Y.-Z. You, C. Xu, A. Vishwanath, A. W. Sandvik, and Z. Y. Meng, Phys. Rev. B **98**, 174421 (2018).
- [10] T. Senthil, arXiv e-prints, arXiv:2306.12638 (2023), arXiv:2306.12638 [cond-mat.str-el].
- [11] A. W. Sandvik, Phys. Rev. Lett. **98**, 227202 (2007).
- [12] J. Lou, A. W. Sandvik, and N. Kawashima, Phys. Rev. B **80**, 180414 (2009).
- [13] K. Harada, T. Suzuki, T. Okubo, H. Matsuo, J. Lou, H. Watanabe, S. Todo, and N. Kawashima, Phys. Rev. B **88**, 220408 (2013).
- [14] A. Nahum, J. T. Chalker, P. Serna, M. Ortuño, and A. M. Somoza, Phys. Rev. X **5**, 041048 (2015).
- [15] H. Shao, W. Guo, and A. W. Sandvik, Science **352**, 213 (2016).
- [16] Y. Nakayama and T. Ohtsuki, Phys. Rev. Lett. **117**, 131601 (2016).
- [17] D. Poland, S. Rychkov, and A. Vichi, Rev. Mod. Phys. **91**, 015002 (2019).
- [18] Z. Li, Bootstrapping conformal qed₃ and deconfined quantum critical point (2022), arXiv:1812.09281 [hep-th].
- [19] A. B. Kuklov, M. Matsumoto, N. V. Prokof'ev, B. V. Svistunov, and M. Troyer, Phys. Rev. Lett. **101**, 050405 (2008).
- [20] K. Chen, Y. Huang, Y. Deng, A. B. Kuklov, N. V. Prokof'ev, and B. V. Svistunov, Phys. Rev. Lett. **110**, 185701 (2013).
- [21] B. Zhao, J. Takahashi, and A. W. Sandvik, Phys. Rev. Lett. **125**, 257204 (2020).
- [22] J. Takahashi, H. Shao, B. Zhao, W. Guo, and A. W. Sandvik, So(5) multicriticality in two-dimensional quantum magnets (2024), arXiv:2405.06607 [cond-mat.str-el].
- [23] R. K. Kaul and A. W. Sandvik, Phys. Rev. Lett. **108**, 137201 (2012).
- [24] M. S. Block, R. G. Melko, and R. K. Kaul, Phys. Rev. Lett. **111**, 137202 (2013).
- [25] M. Song, J. Zhao, Z. Y. Meng, C. Xu, and M. Cheng, arXiv e-prints, arXiv:2312.13498 (2023), arXiv:2312.13498 [cond-mat.str-el].
- [26] M. Song, J. Zhao, M. Cheng, C. Xu, M. M. Scherer, L. Janssen, and Z. Y. Meng, arXiv e-prints, arXiv:2307.02547 (2023), arXiv:2307.02547 [cond-mat.str-el].
- [27] V. Y. Irkhin, A. A. Katanin, and M. I. Katsnelson, Phys. Rev. B **54**, 11953 (1996).
- [28] S. Sachdev, Nature Physics **4**, 173 (2008).
- [29] B. Ihrig, N. Zerf, P. Marquard, I. F. Herbut, and M. M. Scherer, Phys. Rev. B **100**, 134507 (2019).
- [30] A. Nahum, P. Serna, J. T. Chalker, M. Ortuño, and A. M. Somoza, Phys. Rev. Lett. **115**, 267203 (2015).
- [31] J. Lee and S. Sachdev, Phys. Rev. Lett. **114**, 226801 (2015).
- [32] M. Ippoliti, R. S. K. Mong, F. F. Assaad, and M. P. Zaletel, Phys. Rev. B **98**, 235108 (2018).
- [33] Z. Wang, M. P. Zaletel, R. S. K. Mong, and F. F. Assaad, Phys. Rev. Lett. **126**, 045701 (2021).
- [34] P. Di Francesco, P. Mathieu, and D. Sénéchal, *Conformal field theory*, Graduate texts in contemporary physics (Springer, New York, NY, 1997).
- [35] S. Rychkov, *EPFL Lectures on Conformal Field Theory in $D \geq 3$ Dimensions* (Springer International Publishing, 2017).
- [36] J. L. Cardy, Nuclear Physics B **270**, 186 (1986).
- [37] F. D. M. Haldane, Phys. Rev. Lett. **51**, 605 (1983).
- [38] M. Arciniaga and M. R. Peterson, Phys. Rev. B **94**, 035105 (2016).
- [39] B.-X. Lao and S. Rychkov, SciPost Phys. **15**, 243 (2023).
- [40] L. Herviou, A. Läuchli, and S. Rychkov, Fuzzy sphere study of the 3d o(2) cft: Spectrum, finite size corrections and some ope coefficients (2023).
- [41] L. Hu, Y.-C. He, and W. Zhu, Solving conformal defects in 3d conformal field theory using fuzzy sphere regularization (2023), arXiv:2308.01903 [cond-mat.stat-mech].
- [42] Z. Zhou, D. Gaiotto, Y.-C. He, and Y. Zou, The g -function and defect changing operators from wavefunction overlap on a fuzzy sphere (2024), arXiv:2401.00039 [hep-th].
- [43] S. M. Chester and N. Su, Phys. Rev. Lett. **132**, 111601 (2024).
- [44] N. Ma, P. Weinberg, H. Shao, W. Guo, D.-X. Yao, and A. W. Sandvik, Phys. Rev. Lett. **121**, 117202 (2018).
- [45] N. Ma, Y.-Z. You, and Z. Y. Meng, Phys. Rev. Lett. **122**, 175701 (2019).
- [46] J. M. Luck, Phys. Rev. B **31**, 3069 (1985).
- [47] A. Jellal, Nuclear Physics B **804**, 361 (2008).
- [48] M. Greiter and R. Thomale, Annals of Physics **394**, 33 (2024).

- (2018).
- [49] The spherical Landau level regularization of the $SO(5)$ model, the tensor representation of the $SO(5)$ group and alternative calibration schemes of the energy levels to make connection with related works, are shown in this Supplementary Materials.
 - [50] A. Weichselbaum, *Ann. Phys.* **327**, 2972 (2012).
 - [51] A. Weichselbaum, *Phys. Rev. Research* **2**, 023385 (2020).
 - [52] B. Bruognolo, J.-W. Li, J. von Delft, and A. Weichselbaum, *SciPost Phys. Lect. Notes* , 25 (2021).
 - [53] J. L. Cardy, *Journal of Physics A: Mathematical and General* **17**, L385 (1984).
 - [54] J. L. Cardy and P. Grassberger, *Journal of Physics A: Mathematical and General* **18**, L267 (1985).
 - [55] S. Gazit, F. F. Assaad, S. Sachdev, A. Vishwanath, and C. Wang, *Proceedings of the National Academy of Sciences* **115**, E6987 (2018).
 - [56] H. Shackleton, A. Thomson, and S. Sachdev, *Phys. Rev. B* **104**, 045110 (2021).
 - [57] M. Christos, Z.-X. Luo, H. Shackleton, Y.-H. Zhang, M. S. Scheurer, and S. Sachdev, *Proceedings of the National Academy of Sciences* **120**, e2302701120 (2023).
 - [58] M. Christos, H. Shackleton, S. Sachdev, and Z.-X. Luo, *arXiv e-prints* , arXiv:2402.09502 (2024), arXiv:2402.09502 [cond-mat.str-el].
 - [59] A. Zee, *Group Theory in a Nutshell for Physicists* (Princeton University Press, USA, 2016).
 - [60] S. Sternberg, *Group theory and physics* (1994).

SUPPLEMENTAL MATERIALS FOR EMERGENT CONFORMAL SYMMETRY AT THE MULTICRITICAL POINT OF (2+1)D SO(5) MODEL WITH WEISS-ZUMINO-WITTEN TERM ON SPHERE

In Supplemental Materials Section I, we explain the spherical Landau level regularization of the SO(5) model. In Section II, we discuss the tensor representation of the SO(5) group, in which the irreducible representations with their quantum numbers and degeneracies are explicitly given. In Section III, we present further analysis of the energy spectra if other calibration criteria besides the $\Delta_{J\mu} = 2$ and $\Delta_{\mathcal{T}\mu\nu} = 3$ in the main text are used. The purpose of these alternative analysis is to explore the relation of thus obtained scaling dimensions with other recent related works such as Refs. [22, 43]. In Section IV, we present the detailed derivation of the crossing point analysis of the SO(5) order parameter, employed in our previous work [5].

Section I. SPHERICAL LANDAU LEVEL REGULARIZATION OF SO(5) MODEL

I. A. More on the SO(5) model

Our notation is based on that used in Refs. [1, 5, 32, 33].

We would like to project the SO(5) Hamiltonian onto the lowest Landau level (LLL) of the Haldane sphere. The original Hamiltonian is

$$H_\Gamma = \int d\mathbf{r}_1 d\mathbf{r}_2 U(\mathbf{r}_1, \mathbf{r}_2) [n^0(\mathbf{r}_1)n^0(\mathbf{r}_2) - u \sum_{i=1}^5 n^i(\mathbf{r}_1)n^i(\mathbf{r}_2)], \quad (\text{S1})$$

where $n^i(\mathbf{r}) = \Psi(\mathbf{r})^\dagger \Gamma^i \Psi(\mathbf{r}) - \delta_{i0}$ is a local density operator with $\Psi(\mathbf{r}) := \psi_{\tau\sigma}(\mathbf{r})$ the 4-component Dirac fermion annihilation operator with mixing valley τ and spin σ indices. And $\Gamma^0 = \mathbb{I} \otimes \mathbb{I}$, $\Gamma^i = \{\tau_x \otimes \mathbb{I}, \tau_y \otimes \mathbb{I}, \tau_z \otimes \sigma_x, \tau_z \otimes \sigma_y, \tau_z \otimes \sigma_z\}$ are the 5 mutually anticommuting matrices. Here,

$$U(\mathbf{r}_1, \mathbf{r}_2) = \frac{g_0}{R^2} \delta(|\mathbf{r}_1 - \mathbf{r}_2|) + \frac{g_1}{R^4} \nabla^2 \delta(|\mathbf{r}_1 - \mathbf{r}_2|) \quad (\text{S2})$$

describes the SO(5)-preserving short-range interactions with g_0 and g_1 terms.

I. B. Spherical Landau level

For electrons moving on the surface of a sphere with $4\pi s$ monopole ($2s \in \mathbb{Z}$), the Hamiltonian is $H_0 = \frac{1}{2M_e r^2} \Lambda_\mu^2$, and $\Lambda_\mu = \partial_\mu + iA_\mu$. The eigenstates are quantized into spherical Landau levels with energies $E_n = [n(n+1) + (2n+1)s]/(2M_e r^2)$ and $n = 0, 1, \dots$ the Landau level index. The $(n+1)$ th level is $(2s+2n+1)$ -fold degenerate. We assume all interactions are much smaller than the energy gap between Landau levels, and just consider the lowest Landau level (LLL) $n = 0$, which is $(2s+1)$ -fold degenerate and we denote $N = 2s+1$ as the system size of the problem. The wave-functions of LLL orbital are monopole harmonics

$$\Phi_m(\theta, \phi) = N_m e^{im\phi} \cos^{s+m}(\frac{\theta}{2}) \sin^{s-m}(\frac{\theta}{2}), \quad (\text{S3})$$

with $m = -s, -s+1, \dots, s$ and $N_m = \sqrt{\frac{(2s+1)!}{4\pi(s+m)!(s-m)!}}$.

I. C. Details on the LLL projection

The projection of H_Γ on the LLL of the Haldane sphere is carried out as

$$H_\Gamma^{(LLL)} = \int d\mathbf{r}_1 d\mathbf{r}_2 U(\mathbf{r}_1, \mathbf{r}_2) \sum_{m_1, n_1} \Phi_{m_1}^*(\mathbf{r}_1) \Phi_{n_1}(\mathbf{r}_1) \sum_{m_2, n_2} \Phi_{m_2}^*(\mathbf{r}_2) \Phi_{n_2}(\mathbf{r}_2) \times \quad (\text{S4})$$

$$(\sum_{\alpha} c_{m_1, \alpha}^\dagger c_{n_1, \alpha} - 2\delta_{m_1, n_1}) (\sum_{\alpha} c_{m_2, \alpha}^\dagger c_{n_2, \alpha} - 2\delta_{m_2, n_2}) - u \sum_{i=1}^5 (\sum_{\alpha, \beta} c_{m_1, \alpha}^\dagger \Gamma_{\alpha, \beta}^i c_{n_1, \beta}) (\sum_{\alpha, \beta} c_{m_2, \alpha}^\dagger \Gamma_{\alpha, \beta}^i c_{n_2, \beta}) \quad (\text{S5})$$

According to the Legendre polynomial $U(|\mathbf{r}_1 - \mathbf{r}_2|) = \sum_{l=0}^{\infty} U_l P_l(\cos(\Omega_{12})) = \sum_l U_l \frac{4\pi}{2l+1} \sum_{m=-l}^l Y_{l,m}^*(\Omega_1) Y_{l,m}(\Omega_2)$. We then arrive at the form,

$$\begin{aligned}
H_{\Gamma}^{(LLL)} &= \sum_{l,m} U_l \sum_{m_1,m_2} (-1)^{2s+m+m_1+m_2} \frac{(2s+1)^2}{2} \begin{pmatrix} s & l & s \\ -m_1 & -m & m_1+m \end{pmatrix} \begin{pmatrix} s & l & s \\ -m_2 & m & m_2-m \end{pmatrix} \begin{pmatrix} s & l & s \\ -s & 0 & s \end{pmatrix}^2 \\
&\quad \times \left(\sum_{\alpha} c_{m_1,\alpha}^{\dagger} c_{n_1,\alpha} - 2\delta_{m_1,n_1} \right) \left(\sum_{\alpha} c_{m_2,\alpha}^{\dagger} c_{n_2,\alpha} - 2\delta_{m_2,n_2} \right) - u \sum_{i=1}^5 \left(\sum_{\alpha,\beta} c_{m_1,\alpha}^{\dagger} \Gamma_{\alpha,\beta}^i c_{n_1,\beta} \right) \left(\sum_{\alpha,\beta} c_{m_2,\alpha}^{\dagger} \Gamma_{\alpha,\beta}^i c_{n_2,\beta} \right) \\
&= \sum_{m_1,m_2,m} V_{m_1,m_2,m_2-m,m_1+m} \\
&\quad \times \left(\sum_{\alpha} c_{m_1,\alpha}^{\dagger} c_{n_1,\alpha} - 2\delta_{m_1,n_1} \right) \left(\sum_{\alpha} c_{m_2,\alpha}^{\dagger} c_{n_2,\alpha} - 2\delta_{m_2,n_2} \right) - u \sum_{i=1}^5 \left(\sum_{\alpha,\beta} c_{m_1,\alpha}^{\dagger} \Gamma_{\alpha,\beta}^i c_{n_1,\beta} \right) \left(\sum_{\alpha,\beta} c_{m_2,\alpha}^{\dagger} \Gamma_{\alpha,\beta}^i c_{n_2,\beta} \right)
\end{aligned} \tag{S6}$$

with

$$V_{m_1,m_2,m_3,m_4} = (-1)^{2s+m_1+2m_2-m_3} \frac{(2s+1)^2}{2} \sum_l U_l (2l+1) \begin{pmatrix} s & l & s \\ -m_1 & m_1-m_4 & m_4 \end{pmatrix} \begin{pmatrix} s & l & s \\ -m_2 & m_2-m_3 & m_3 \end{pmatrix} \begin{pmatrix} s & l & s \\ -s & 0 & s \end{pmatrix}^2. \tag{S7}$$

I. D. Connection to Haldane's pseudo-potential

In this part, we discuss the interaction we considered [c.f. Eq. (S2)] and its relation with the Haldane's pseudopotential V_l . The form factor V_{m_1,m_2,m_3,m_4} [c.f. Eq. (S7)] is connected to V_l by

$$V_{m_1,m_2,m_3,m_4} = \sum_l V_l (4s-2l+1) \begin{pmatrix} s & s & 2s-l \\ m_1 & m_2 & -m_1-m_2 \end{pmatrix} \begin{pmatrix} s & s & 2s-l \\ m_4 & m_3 & -m_4-m_3 \end{pmatrix}. \tag{S8}$$

The relation between U_l and V_l is then given by,

$$V_{2s-l} = (-1)^{2s+l} \sum_k U_k \begin{pmatrix} s & k & s \\ -s & 0 & s \end{pmatrix}^2 \begin{Bmatrix} s & s & l \\ s & s & k \end{Bmatrix}. \tag{S9}$$

To be specific, for the short-range interaction $U(\mathbf{r}_1, \mathbf{r}_2) = \frac{g_0}{R^2} \delta(|\mathbf{r}_1 - \mathbf{r}_2|) + \frac{g_1}{R^4} \nabla^2 \delta(|\mathbf{r}_1 - \mathbf{r}_2|)$, only the contact interaction of the form of delta function and its derivatives are considered, and only V_0 and V_1 are involved in the Haldane's pseudopotential. And the relations between (g_0, g_1) and (V_0, V_1) is given by

$$V_l = \begin{cases} \frac{g_0(2s+1)-g_1s}{4s+1}, & \text{if } l = 0 \\ \frac{g_1s}{4s-1}, & \text{if } l = 1. \end{cases} \tag{S10}$$

Section II. TENSOR REPRESENTATION OF $\text{SO}(N)$ GROUP

In this section, we briefly recapitulate basic conclusions of $\text{SO}(N)$ group and its irreducible representation [59, 60]. These information forms the foundation upon which we classify the energy levels in the ED and DMRG simulations of the $\text{SO}(5)$ model with WZW term.

By definition, the $\text{SO}(N)$ group is the group of all $N \times N$ matrices R satisfying $R^T R = I$ (orthogonal condition) and $\det(R) = 1$. These $N \times N$ matrices thus form the defining representation, furnished by N -dimensional vectors.

To systematically construct representations with larger dimensions, one needs more complicated objects than vectors, i.e., a rank- j tensor denotes as $T^{\mu_1 \mu_2 \dots \mu_j}$ with j indices, where μ_j can take the N integers. It transforms as

$$\tilde{T}^{\nu_1 \nu_2 \dots \nu_j} = R_{\mu_1}^{\nu_1} R_{\mu_2}^{\nu_2} \dots R_{\mu_j}^{\nu_j} T^{\mu_1 \mu_2 \dots \mu_j}.$$

The number of elements in rank- j tensor $T^{\mu_1\mu_2\cdots\mu_j}$ is N^j , and such generic rank- j tensors thus furnish a $N^j \times N^j$ representation, which generally speaking is reducible. To be specific, it can be decomposed into sectors with different index symmetries.

For instance, a rank-2 tensor can be decomposed as the symmetric part and the anti-symmetric part, i.e., $T^{ij} = S^{ij} + A^{ij}$, where $S^{ij} = (T^{ij} + T^{ji})/2$ is a symmetric tensor and $A^{ij} = (T^{ij} - T^{ji})/2$ is a anti-symmetric tensor. It is straightforward to check such index permutation symmetries are preserved under $SO(N)$ transformations. That is, a subset of tensors with a given index symmetry constitute an invariant subspace. Note that, the trace of a tensor remains the same under $SO(N)$ rotation, which means that, the symmetric tensor can be further decomposed into the traceless symmetric tensor and the trace itself. To sum up, for rank-2 tensors, the N^2 -dimensional space can be decomposed into, a $(N(N+1)/2 - 1)$ -dimensional invariant subspace (furnished by the traceless symmetric tensors), a $N(N-1)/2$ -dimensional invariant subspace (furnished by the anti-symmetric tensors), and a one-dimensional invariant subspace (by the trace of the rank-2 tensors), denoted as,

$$N^2 = \frac{N(N+1)}{2} - 1 \oplus \frac{N(N-1)}{2} \oplus 1.$$

For $SO(5)$ group, this means

$$25 = 14 \oplus 10 \oplus 1.$$

For more complicated symmetries in higher rank tensors, one usually resorts to the simple yet powerful tools of the Young tableaux, where each tableau represents a specific process of symmetrization and anti-symmetrization for the indices of the tensor $T^{\mu_1\mu_2\cdots\mu_j}$ [60]. In practice, one first fill in all indices into a given Young diagram $[\lambda]$, then symmetrizes all indices for each row and anti-symmetrizes all indices for each column. For instance, the Young diagram

$$\begin{array}{|c|c|} \hline \mu & \rho \\ \hline \nu & \\ \hline \end{array}$$

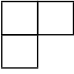
$[2, 1]$, depicted as $\begin{array}{|c|c|} \hline \mu & \rho \\ \hline \nu & \\ \hline \end{array}$, represents the mix-symmetry rank-3 tensors $M^{\mu\rho\nu} = (T^{\nu\mu\rho} + T^{\nu\rho\mu}) - (T^{\mu\nu\rho} + T^{\mu\rho\nu})$. The dimension of a tensor representation can be given by the Young tableaux theory. When the number of rows in a given Young diagram $[\lambda]$ is not equal to $N/2$ (applied to the considered $N = 5$ case here), the dimension is then given by the ratio of two tableaux $\frac{Y_T^{[\lambda]}}{Y_h^{[\lambda]}}$. Here the denominator tableaux $Y_h^{[\lambda]}$ is simply given by filling in the hook length h_{ij} into the box of the i -th row and j -th column, and calculating their product. The numerator tableaux $Y_T^{[\lambda]}$ is slightly more complicated, where for a given box the number filled is the sum of that in the corresponding box of a set of tableaux $\{Y_{T_a}^{[\lambda]}\}$. The rules to write down the series of $Y_{T_a}^{[\lambda]}$ are as follows.

1. Tableaux $Y_{T_0}^{[\lambda]}$ is given by filling $N - i + j$ into the box at the i -th row and j -th column;
2. Let $[\lambda^1] = [\lambda]$. We then define a series of diagram $[\lambda^a]$ by removing the first row and column of the diagram $[\lambda^{a-1}]$, until the number of columns is less than 2.
3. Given diagram $[\lambda^a]$, for the first- r boxes (with r being the row of $[\lambda^a]$) of the hook $(1, 1)$, we successively fill in $(\lambda_1^a - 1), (\lambda_2^a - 1), \dots, (\lambda_r^a - 1)$. For each hook $(i, 1)$ with $1 \leq i \leq r$, we fill (-1) into the last- $(\lambda_i^a - 1)$ boxes.

This ends the definition of tableaux $Y_{T_a}^{[\lambda]}$.

For the $SO(5)$ group we considered in the main text, a few of the lowest-dimensional representations (without spinor) are listed as follows.



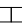
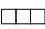
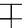
1. $\begin{array}{|c|} \hline \\ \hline \end{array}$ (rank-1 tensor, the vector representation): the dimension is $\frac{5}{1} = \frac{5}{1} = 5$;
2. $\begin{array}{|c|c|} \hline & \\ \hline \end{array}$ (the traceless symmetric rank-2 tensor): the dimension is $\frac{\begin{array}{|c|c|} \hline 5 & 6 \\ \hline 2 & 1 \end{array} + \begin{array}{|c|} \hline -1 \\ \hline \end{array}}{\begin{array}{|c|} \hline 2 \\ \hline 1 \end{array}} = \frac{\begin{array}{|c|c|} \hline 4 & 7 \\ \hline 2 & 1 \end{array}}{\begin{array}{|c|} \hline 2 \\ \hline 1 \end{array}} = \frac{4 \times 7}{2 \times 1} = 14$;
3. $\begin{array}{|c|} \hline \\ \hline \end{array}$ (the anti-symmetric rank-2 tensor): the dimension is $\frac{\begin{array}{|c|} \hline 5 \\ \hline 4 \\ \hline 2 \\ \hline 1 \end{array}}{\begin{array}{|c|} \hline 2 \\ \hline 1 \end{array}} = \frac{5 \times 4}{2 \times 1} = 10$;
4. $\begin{array}{|c|c|c|} \hline & & \\ \hline \end{array}$ (the fully symmetric rank-3 tensor): the dimension is $\frac{\begin{array}{|c|c|c|} \hline 5 & 6 & 7 \\ \hline 3 & 2 & 1 \end{array} + \begin{array}{|c|} \hline -1 \\ \hline \end{array} + \begin{array}{|c|} \hline -1 \\ \hline \end{array} + \begin{array}{|c|} \hline 2 \\ \hline \end{array}}{\begin{array}{|c|} \hline 3 \\ \hline 2 \\ \hline 1 \end{array}} = \frac{\begin{array}{|c|c|c|} \hline 4 & 5 & 9 \\ \hline 3 & 2 & 1 \end{array}}{\begin{array}{|c|} \hline 3 \\ \hline 2 \\ \hline 1 \end{array}} = \frac{4 \times 5 \times 9}{3 \times 2 \times 1} = 30$;

5.  (the mixed-symmetry rank-3 tensor): the dimension is $\frac{\begin{smallmatrix} 5 & 6 \\ 4 \end{smallmatrix} + \begin{smallmatrix} 0 & 1 \\ -1 \end{smallmatrix}}{\begin{smallmatrix} 3 & 1 \\ 1 \end{smallmatrix}} = \frac{\begin{smallmatrix} 5 & 7 \\ 3 \end{smallmatrix}}{\begin{smallmatrix} 3 & 1 \\ 1 \end{smallmatrix}} = \frac{5 \times 7 \times 3}{3 \times 1 \times 1} = 35;$

6. etc.



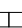
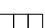
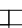
In our ED calculation, we have the conserved quantum numbers, the z -component of the total spin σ^z , the total valley τ^z , the total charge number q^z . The tensor representations manifest themselves through the degeneracies in each (σ^z, τ^z, q^z) sector. As shown in Tab. S1 we list the SO(5) representations and their corresponding degeneracies in $(\sigma^z, \tau^z, q^z = 2(2s + 1))$ sectors. Here, we only list the sectors with $\sigma^z \geq 0$ and $\tau^z \geq 0$, and the sectors $(\pm\sigma^z, \pm\tau^z)$ should have the same degeneracy.

TABLE S1. The Young diagrams of different SO(5) irreducible representations (denoted as IREP) and the corresponding state degeneracies in different (σ^z, τ^z) sectors.

SO(5) IREP	Young diagram	(0,0)	(0,2)	(0,4)	(0,6)	(2,0)	(2,2)	(2,4)	(4,0)	(4,2)	(6,0)
1		1									
5		1	1			1					
10		2	1			1	1				
14		2	1	1		1	1		1		
30		2	2	1	1	2	1	1	1	1	1
35		3	3	2		3	2	1	1	1	

In our DMRG calculation, we have the conserved quantum numbers, the total spin S , the total charge number q^z . The tensor representations manifest themselves through the degeneracies in each (S, q^z) sector. As shown in Tab. S2 we list the SO(5) representations and their corresponding degeneracies in $(S, q^z = 2(2s + 1))$ sectors.

TABLE S2. The Young diagrams of different SO(5) irreducible representations (denoted as IREP) and the corresponding state degeneracies in different sectors with total spin S at half-filling case $q^z = 2(2s + 1)$.

SO(5) IREP	Young diagram	0	1	2	3
1		1			
5		2	3		
10		1	9		
14		3	6	5	
30		4	9	10	
35		2	18	15	

Section III. ANALYSIS OF RECALIBRATED SPECTRUM

In the main text, we use the criteria of $\Delta_{J\mu} = 2$ and $\Delta_{\mathcal{T}\mu\nu} = 3$ to determine the microscopic parameter at which the CFT energy level structure is revealed. As shown in Tab. S3, we list our obtained scaling dimensions of several operators, namely, the order parameter Δ_ϕ , singlet operator Δ_S , the lowest rank-2 tensor Δ_T , and the symmetry current $\Delta_{J\mu}$, together with the recent conformal bootstrap data assuming tricritical point [43], a recent ED study of the same SO(5) model we consider in fuzzy sphere [4], and a recent QMC study of J - Q model [22].

As shown in the main text, the analysis still has noticeable finite size effect even if we tune the length of the interaction. In this section, we try to loose the constraints of $\Delta_{J\mu} = 2$ and $\Delta_{\mathcal{T}\mu\nu} = 3$ on the finite size data, and test

TABLE S3. Scaling dimension of relevant primary operator at $V_1 = 0.3$ and those from related works.

Operators	ϕ	S	T	J^μ
This work	0.646	2.884	1.633	2.000*
Conformal Bootstrap tricritical point [43]	0.630*	2.359	1.519	2.000*
Fuzzy sphere with SO(5) symmetry only and $V_1 = 0$ [4]	0.585	2.831	1.458	2.000*
J - Q model [22]	0.607(4)	2.273(4)	1.417(7)	2.01(3)

our energy levels with other criteria in such a way that, given the recent relevant work from the conformal bootstrap analysis of the deconfined quantum tricriticality [43], and Quantum Monte Carlo simulation of J - Q model [22], how large is the degree of freedom our obtained scaling dimensions are consistent with these other results.

As shown in Tab. S4, for the cases of $V_1 = 0.3$, we instead calibrate our energy spectrum to make the scaling dimension of symmetry current $\Delta_J = 2$ and order parameter $\Delta_\phi = 0.630$ (the one taken in the conformal bootstrap work [43]). It can be seen that, when $V_1 = 0.3$, the rank-2 tensor has a scaling dimension of 1.593 which is closer to the value of 1.519 given by the conformal bootstrap, whereas the singlet operator is 2.774 which is far from 2.359.

TABLE S4. Scaling dimensions of relevant primary operators at $V_1 = 0.3$ for various system sizes N when recalibrating the operator spectrum to make $\Delta_J = 2$ and $\Delta_\phi = 0.630$ (the one taken in conformal bootstrap [43]).

	Op.				
	ϕ	T	S	J^μ	$\mathcal{T}^{\mu\nu}$
$N = 4$	0.630*	1.590	2.777	2.000*	3.047
$N = 5$	0.630*	1.592	2.774	2.000*	3.042
$N = 6$	0.630*	1.593	2.780	2.000*	3.046
Conformal Bootstrap tricritical point [43]	0.630*	1.519	2.359	2.000*	—

TABLE S5. Scaling dimensions of relevant primary operators at $V_1 = 0.3$ for various system sizes N when recalibrating the operator spectrum to make $\Delta_J = 2$ and $\Delta_\phi = 0.607$ (the one obtained in J - Q model [22]).

	Op.				
	ϕ	T	S	J^μ	$\mathcal{T}^{\mu\nu}$
$N = 4$	0.607*	1.531	2.688	2.000*	3.133
$N = 5$	0.607*	1.533	2.681	2.000*	3.121
$N = 6$	0.607*	1.533	2.684	2.000*	3.121
J - Q model [22]	0.607(4)	1.417(7)	2.273(4)	2.01(3)	—

As shown in Tab. S5, for the cases of $V_1 = 0.3$, we also calibrate our energy spectrum to make the scaling dimension of symmetry current $\Delta_J = 2$ and order parameter $\Delta_\phi = 0.607$ (the one obtained in the J - Q model [22]). It can be seen that, when $V_1 = 0.3$, the rank-2 tensor has a scaling dimension of 1.533 which is closer to the value of 1.417 obtained in the J - Q model, whereas the singlet operator is 2.684 which is far from 2.273.

Based on these analyses, we conclude that all these recent works on existence of the multicritical point of the SO(5), although still differ at the second/third significant digit, but they reveal the consistent picture that for the SO(5) CFT we find in this work, there exists two relevant singlets, the Δ_S and Δ_T , whose scaling dimensions are both smaller than 3. And by tuning $V_1 = 0.3$ and calibrate with Δ_ϕ taken in the conformal bootstrap work [43] and obtained in the QMC study of J - Q model [22], we observe the Δ_s become closer to the bootstrap value and the J - Q value. Such analysis supports the conclusion that the emergent CFT we have discovered, along with those from other related works, is a multicritical point.

Section IV. CROSSING POINT ANALYSIS

In this section, we provide the detailed derivation for the scaling form of the crossing points, such that the position of the critical point and the associated scaling dimension can be obtained in a controlled manner from the finite size data. Such crossing point analysis has been widely applied and tested for quantum criticality of 2D Ising, SU(2) and other spin models [8, 15, 44, 45] and can be further traced back to Fisher's "phenomenological renormalization",

which was first numerically tested with transfer matrix results for the Ising model in Ref. [46]. It has been used in our previous work [5] to determine the SO(5) phase diagram.

Let's consider the standard form of finite-size scaling for an arbitrary observable,

$$O(\delta, L) = L^{-\kappa/\nu} f(\delta L^{1/\nu}, \lambda L^{-\omega}). \quad (\text{S11})$$

Here, $\delta = q - q_c$ is the deviation from the transition point q_c , and we also consider the correction from the leading irrelevant field λ and its corresponding exponent ω . In practise, due to the limit of computational resources, we only increase the system size by x , and consider the crossing point of observable between size pair $(N, N+x)$. For the sake of notation simplicity, we express the scaling form as a function of total number of size N instead of linear size $L \sim \sqrt{N}$, i.e.,

$$O(\delta, N) = N^{-\frac{\kappa}{2\nu}} f(\delta N^{\frac{1}{2\nu}}, \lambda N^{-\frac{\omega}{2}}) = N^{-\frac{\kappa}{2\nu}} (a_0 + a_1 \delta N^{\frac{1}{2\nu}} + b_1 N^{-\frac{\omega}{2}} + \dots), \quad (\text{S12})$$

where the second equality relation is simply from Taylor's expansion up to first-order. Similarly, for system size $N+x$, we have

$$O(\delta, N+x) = (N+x)^{-\frac{\kappa}{2\nu}} (a_0 + a_1 \delta (N+x)^{\frac{1}{2\nu}} + b_1 (N+x)^{-\frac{\omega}{2}} + \dots). \quad (\text{S13})$$

Then, at the crossing point δ^* , by definition we have $O(\delta^*, N) = O(\delta^*, N+x)$, which leads to the scaling form for the crossing point itself and the observable at the crossing point,

$$\delta^*(N) = \frac{a_0}{a_1} \frac{(1+x/N)^{-\frac{\kappa}{2\nu}} - 1}{1 - (1+x/N)^{\frac{1-\kappa}{2\nu}}} N^{-\frac{1}{2\nu}} + \frac{b_1}{a_1} \frac{(1+x/N)^{-\frac{\omega}{2} - \frac{\kappa}{2\nu}} - 1}{1 - (1+x/N)^{\frac{1-\kappa}{2\nu}}} N^{-\frac{1}{2\nu} - \frac{\omega}{2}} + \dots. \quad (\text{S14})$$

In the case of Binder ratio, we have $\kappa = 0$ and when $x \ll N$, we then arrive at

$$\delta^*(N) = a N^{-\frac{1}{2\nu} - \frac{\omega}{2}} + \dots. \quad (\text{S15})$$

From the above scaling form [c.f. Eq. (S15)], in principle, we can fit the finite-size data of the crossing point, from which the critical point can be extracted. In the main text, we applied this method to determine the transition point between the SO(5) symmetry-breaking phase and the symmetric phase.

To determine the scaling dimension of order parameter Δ_ϕ , by considering the order parameter $\phi(\delta, N) = N^{-\frac{\Delta_\phi}{2}} (a_0 + a_1 \delta N^{\frac{1}{2\nu}} + \dots)$, the logarithmic of the order parameter between size pair $(N, N+x)$ will be

$$\log \frac{\phi(\delta, N+x)}{\phi(\delta, N)} = -\frac{\Delta_\phi}{2} \frac{x}{N} + \frac{a_1}{a_0} \delta N^{\frac{1}{2\nu}} \frac{x}{N}. \quad (\text{S16})$$

Then, we can define the finite-size value of $\Delta^*(N)$ as

$$\Delta_\phi^*(N) \equiv -\frac{2N}{x} \log \frac{\phi(\delta, N+x)}{\phi(\delta, N)}, \quad (\text{S17})$$

which will take the scaling form as

$$\Delta_\phi^*(N) = \Delta_\phi + c N^{\frac{1}{2\nu}}, \quad (\text{S18})$$

where both of the sides will take the value of scaling dimension Δ_ϕ when N is extrapolated to 0.